Surface Forces in Solutions Containing Semiflexible Polymers

Jan Forsman*

Theoretical Chemistry, Chemical Centre, P.O. Box 124, S-221 00 Lund, Sweden

Clifford E. Woodward

School of Physical Environmental and Mathematical Sciences, University College, University of New South Wales, Building 22, Australian Defence Force Academy, Canberra ACT 2600, Australia

Received September 5, 2005; Revised Manuscript Received November 18, 2005

ABSTRACT: The influence of intrinsic chain stiffness on surface forces in solutions containing semiflexible polymers is investigated with density functional theory. The solvent is included explicitly, but comparisons are also made with exact results obtained with ideal chains, in the absence of solvent particles. We find that as the intrinsic stiffness increases, the polymers are at intermediate separations less able to form strong attractive bridges. This leads to a substantial free energy barrier. At short separations, bridging does dominate, resulting in an attractive interaction. However, the way in which the height of the free energy barrier responds to changes of the chain length, at a given stiffness, as well as on stiffness, for a given chain length, is nontrivial and not monotonic. There is furthermore a saturation effect, which at high monomer concentrations leads to a depletion interaction at intermediate separations. This amounts to a reversal of the mechanisms underlying the net interaction. That the density functional theory is accurate is verified by an excellent agreement between predicted structural properties and corresponding data obtained by simulations.

1. Introduction

The stability of colloid polymer mixtures has been studied both experimentally[1−7] and theoretically.[8−21] In a series of articles[22−25] we have studied the influence of polymer solutions on the interactions between surfaces, using density functional theory. The qualitative behavior of these surface forces depends on the nature of the interactions between surfaces and monomer and solvent particles, the monomer−solvent interactions, and also the intramolecular structure of the polymer molecules. In this work, we will study surfaces that are attractive to a solution of polymer molecules with some degree of internal stiffness. This is a logical progression from the completely flexible polymer models that we have considered in our past investigations.

In an early treatment, de Gennes[12,13] used self-consistent-field theory to study adsorbing surfaces in the presence of a solution containing flexible polymers. The ground state dominance approximation was made,[26] which assumes an infinite length for the polymer molecules. As discussed recently by Blokhuis et al.,[27] this approximation fails to capture an important aspect of surface forces, which are related to finite chain lengths. Mean-field calculations on polymer-induced depletion forces and weakly adsorbing surfaces show that the relevant length scale over which the surface forces act will be the radius of gyration for very dilute solutions, switching to the *bulk correlation length* above the overlap concentration. The theory of de Gennes predicts a monotonic attraction for adsorbing surfaces. This is to be contrasted with more general mean-field treatments, in which polymer size effects are included.[19,23,27] These predict nonmonotonic behavior of the surface forces, with weak repulsive free energy barriers preceding an attractive regime at short separations. These repulsions has been suggested to be due to protruding tails, which are absent in the ground-state dominant approximation. In this work, we explore interactions between surfaces that contain semiflexible polymers of finite length. These will be moderately stiff in the sense that the persistence length is considerably smaller than the fully stretched polymer. We will focus on the relation between chain rigidity and surface forces. Recent theoretical works[28−31] on semiflexible polymer solutions have focused on polymer adsorption at single surfaces, using both Monte Carlo simulations and mean-field theories. Very little systematic work has been done on surface forces in these systems. The density functional theory that we have used in previous studies on flexible polymer solutions is generalized here to include the presence of an angular dependent potential, between adjacent monomer bonds. This potential is parametrized, enabling surface forces to be monitored as the intramolecular stiffness is varied. The functional has already been used by Forsman and Woodward[32] to improve the description of polymer fluids at low concentrations. In an earlier work,[33] Yethiraj and Woodward investigated semiflexible polymer solutions between inert surfaces. Their approach included mean-field single-chain Monte Carlo simulations to solve variational equations, which proved relatively time-consuming, but still much more efficient than full Monte Carlo or molecular dynamics simulations. In this work, we have implemented a completely self-contained numerical solution of the density functional equations, by fully reducing the dimensional dependence of the angular component of the intramolecular potential. In addition, a more versatile excess free energy functional, based on an equation of state by Wichert et al.,[22,34] is used. This functional is able to treat models where monomers and solvent particles have different size. The accuracy of the density functional theory is evaluated in the Appendix, which contains structural comparisons with simulation data.

Many theoretical models of polymer solutions are based on an implicit treatment of the solvent. Often, these use effective "solvent-induced" interactions between monomers as well as an assumption of solution incompressibility. This is not always an adequate description of the system.[22,23] In the system we

* Corresponding author. E-mail: jan.forsman@teokem.lu.se.

10.1021/ma051934g CCC: $33.50
Published on Web 01/04/2006

study here, for example, there are significant density structure effects that are exhibited by both monomer and solvent particles, which cannot be captured by an implicit solvent model. In this work, polymer solutions are fully described with an *explicit* treatment of the solvent particles. The results of these calculations are compared to those of ideal polymer fluids, i.e., polymer fluids in which there are no monomer−monomer interactions, except for nearest-neighbor bonds and the effective next-nearest-neighbor repulsion that results from the bond angle potential (stiffness potential). An important virtue of these ideal systems is that the density functional treatment of these fluid is *exact*, and the integrals can in principle be solved to any desired degree of accuracy. In practice, the partitioning used when solving these integrals is so dense that the results for these systems indeed can be regarded as exact.

2. Polymer Solution Model and Density Functional Theory

We shall give a brief outline of the density functional theory here. More detailed descriptions can be found elsewhere.[22,24,35] Our model consists of polymer molecules, each containing r monomers, and solvent particles. Both solvent particles and monomers are hard spheres with the same diameter, σ, though the theory is in principle able to treat different sized particles as well. The configuration of a polymer molecule is represented as, $\mathbf{R} = (\mathbf{r}_1,...,\mathbf{r}_r)$, where $\boldsymbol{r}_i$ is the coordinate of monomer i. The total bonding potential is given by $V_b(\mathbf{R})$. This potential defines the architecture of the polymer chains, i.e., linear or star shaped, as well as chain stiffness (which will be described in the next section). For a fully flexible linear polymer, the bonding potential has the form

$$e^{-\beta V_b(\mathbf{R})} \propto \prod_{i=1}^{r-1} \delta(|\mathbf{r}_{i+1} - \mathbf{r}_i| - \sigma) \tag{1}$$

where $\delta(x)$ is the Dirac delta function and $\beta = 1/(k_B T)$ is the inverse thermal energy. The multipoint polymer density distribution is denoted by $N(\mathbf{R})$; i.e., $N(\mathbf{R})\ d\mathbf{R}$ is the number of polymer molecules having configurations between $\mathbf{R}$ and $\mathbf{R} + d\mathbf{R}$. For a fluid of ideal chains, the *exact* expression for the free energy functional, $\mathcal{F}_p^{id}$, is[35]

$$\beta\mathcal{F}_p^{id}[N(\mathbf{R})] = \int N(\mathbf{R})(\ln[N(\mathbf{R})] - 1)\, d\mathbf{R} + \beta \int N(\mathbf{R})\, V_b(\mathbf{R})\, d\mathbf{R} \tag{2}$$

The total free energy will contain ideal terms from the solvent as well as excess contributions due to hard-sphere interactions between the fluid particles. A general expression for the grand potential, Ω, can be written as[35]

$$\beta\Omega[N(\mathbf{R}), n_s(\mathbf{r})] = \beta\mathcal{F}_p^{id}[N(\mathbf{R})] + \int n_s(\mathbf{r})(\ln[n_s(\mathbf{r})] - 1)\, d\mathbf{r} + \beta\mathcal{F}^{ex}[\bar{n}_m(\mathbf{r}), \bar{n}_s(\mathbf{r})] + \int \beta(V_m^{ext}(\mathbf{r}) - \mu_p) n_m(\mathbf{r})\, d\mathbf{r} + \int \beta(V_s^{ext}(\mathbf{r}) - \mu_s) n_s(\mathbf{r})\, d\mathbf{r} \tag{3}$$

where μ_p and μ_s are the polymer and solvent chemical potentials, respectively. In this expression we have written the interaction with the external potential in terms of the monomer and solvent particle densities, denoted by $n_s(\mathbf{r})$ and $n_m(\mathbf{r})$, respectively. $V_\alpha^{ext}(\mathbf{R})$ is an external potential acting on particle species α (solvent or monomer). $\mathcal{F}^{ex}[\bar{n}_m(\mathbf{r}),\bar{n}_s(\mathbf{r})]$ is the excess free energy which describes interactions between all particles (monomers and solvent) in the solution. For instance, the overlap between chains adsorbed on approaching opposing surfaces is taken into account via the increased monomer density that results from such an overlap. This leads to an increased mean-field "penalty", expressed as $\delta\mathcal{F}^{ex}/\delta n_m$, which generates a repulsion (in hard-core systems) and regulates the monomer increase (to a value below the corresponding one for ideal chains, provided there are no attractive interactions).

In this work, $\mathcal{F}^{ex}$ is obtained from an approximate equation of state. However, a formal analysis of density functional theory shows that in principle it is possible to construct an exact functional that has a similar *form* to the functional described here. A more detailed description of the density functional theory can be found in ref 35.

Forsman et al.[22,24] have derived an expression for the excess part of the functional, by integrating an equation of state developed by Wichert et al.[34] The coarse-grained densities, $\bar{n}_s(\mathbf{r})$ and $\bar{n}_m(\mathbf{r})$, which appear in this functional, are defined by

$$\bar{n}_\alpha(\mathbf{r}) = \frac{3}{4\pi\sigma^3} \int_{|\mathbf{r}-\mathbf{r}'|<\sigma} n_\alpha(\mathbf{r}')\, d\mathbf{r}' \tag{4}$$

with $\alpha = s, m$ denoting solvent particles and monomers, respectively. This nonlocal formulation of the excluded-volume contribution is able to describe nonuniform fluid structures with reasonable accuracy.[36]

In this work we shall study polymer solutions confined by parallel, flat surfaces separated by a distance h. The planar symmetry simplifies the expressions for the density functional significantly, as we need only consider functions which vary in the z-coordinate (perpendicular to the surfaces). The potential $V^{ext}(h,z)$ defines the total interaction between the surfaces and the confined fluid particles:

$$V^{ext}(z) = w(z) + w(h - z) \tag{5}$$

In this work we shall assume that the surface interaction does not discriminate between solvent and monomer particles. The contribution from each wall is

$$w(z) = A_w e^{-z/\tau} w_{L-J}(z) \tag{6}$$

The function $w_{L-J}(z)$ is the usual Lennard-Jones wall interaction

$$\beta w_{L-J}(z) = 2\pi\left[\frac{2}{45}\left(\frac{\sigma}{z}\right)^9 - \frac{1}{3}\left(\frac{\sigma}{z}\right)^3\right] \tag{7}$$

This surface potential is the same form as used in our previous work.[23,25] In the present study, we have fixed the value of the decay length, τ: $\tau/\sigma = 1$, giving rise to a rather short-ranged surface interaction. The strength of the adsorption potential is determined by the parameter A_w. For polymer solutions, we have used the same value as in our previous studies,[23] i.e., $A_w \approx 2.7057$. For ideal chains, this leads to unphysically strong adsorption, and we have therefore chosen a smaller value for these systems: $A_w = 0.9$.

2.1. Stiff Polymers. A semiflexible polymer molecule can be modeled by the introducing a bending potential between next-nearest neighbors. Let $\mathbf{s}_i$ denote the bond vector between monomers i and $i + 1$. The bending potential, E_b, is given by the following equation:

$$\beta E_b = \epsilon\left(1 - \frac{\mathbf{s}_i \mathbf{s}_{i+1}}{\sigma^2}\right) \tag{8}$$

The strength of this potential is determined by the parameter, ϵ. The vector product is written as

$$\mathbf{s}_i\mathbf{s}_{i+1} = \Delta z_i \Delta z_{i+1} + (\sigma^2 - \Delta z_i^2)^{1/2}(\sigma^2 - \Delta z_{i+1}^2)^{1/2}\cos\Phi_{i,i+1} \quad (9)$$

where $\Phi_{i,i+1}$ is the angle between the bond vectors $\mathbf{s}_i$ and $\mathbf{s}_{i+1}$, projected onto the plane of the surfaces. Furthermore, $\Delta z_i \equiv z_{i+1} - z_i$, where z_i is the z coordinate of monomer i. Averaging the Boltzmann factor containing this bending potential over the surface plane (i.e., averaging over the projected angle) gives

$$\Psi(\Delta z_i,\Delta z_{i+1}) \equiv \int\int \mathrm{e}^{-\beta E_b}\,\mathrm{d}x\,\mathrm{d}y = \begin{cases} \mathrm{e}^{\epsilon(1-(\Delta z_i \Delta z_{i+1})/\sigma^2)} I_0\left[\epsilon\left(1-\left(\frac{\Delta z_i}{\sigma}\right)^2\right)^{1/2}\left(1-\left(\frac{\Delta z_{i+1}}{\sigma}\right)^2\right)^{1/2}\right], & i \le r-2 \\ 1, & i > r-2 \end{cases} \quad (10)$$

where

$$I_0(x) = \frac{1}{2\pi}\int_0^{2\pi} \mathrm{e}^{-x\cos\Phi}\,\mathrm{d}\Phi \quad (11)$$

is the modified Bessel function.

Single chain properties can be readily obtained from this form of the bending potential. For example, the root-mean-square end-to-end separation, $\langle \mathbf{R}_{ee}\mathbf{R}_{ee}\rangle^{1/2}$, can be calculated as

$$\begin{aligned}\frac{\langle \mathbf{R}_{ee}\mathbf{R}_{ee}\rangle}{\sigma^2} &= r - 1 + 2((r-2)\langle\cos(\Phi_{i,i+1})\rangle_\epsilon + (r-3)\langle\cos(\Phi_{i,i+1})\rangle_\epsilon^2 + ...) \\ &= r - 1 + 2\sum_{i=1}^{r-2}(r-1-i)\langle\cos(\Phi_{i,i+1})\rangle_\epsilon^i \\ &= r - 1 + 2\sum_{i=1}^{r-2}(r-1-i)\left[\frac{\mathrm{e}^{-2\epsilon}(1+\epsilon)+\epsilon-1}{\epsilon(1-\mathrm{e}^{-2\epsilon})}\right]^i\end{aligned} \quad (12)$$

where the brackets $\langle ... \rangle_\epsilon$ denote a Boltzmann-weighted orientational average, at the given stiffness parameter, ϵ. The persistence length, $\lambda_p = \langle \mathbf{R}_{ee}\mathbf{s}_1/\sigma\rangle$, is also easily evaluated, in an analogous fashion:

$$\lambda_p/\sigma = \frac{\epsilon(1-\mathrm{e}^{-2\epsilon})}{1-\mathrm{e}^{-2\epsilon}(1+2\epsilon)} \quad (13)$$

Thus, the persistence length can be approximated as $\lambda_p/\sigma \approx \epsilon$, even for moderate values of ϵ.

2.2. Numerical Solution. Upon minimizing the free energy functional, one obtains the following expression for the equilibrium monomer density profile:

$$n_m(z) = \mathrm{e}^{\beta\mu_p}\sum_{i=1}^{r}\int_0^h \delta(z-z_i)\prod_{j=1}^{r}\mathrm{e}^{-\lambda_m(z_j)}\prod_{k=1}^{r-1}\Theta(|\Delta z_k| - \sigma) \times \prod_{l=1}^{r-2}\Psi(\Delta z_l,\Delta z_{l+1})\,\mathrm{d}z_1 ... \mathrm{d}z_r \quad (14)$$

where

$$\lambda_m(z) = \frac{\partial \beta F_{\mathrm{ex}}}{\partial n_m(z)} \quad (15)$$

and $\Theta(x)$ is the Heaviside step function

$$\Theta(x) = \begin{cases} 1, & x \le 0 \\ 0, & x > 0 \end{cases} \quad (16)$$

The solution to eq 14 can be obtained via a Picard iteration scheme, as has already been outlined in ref 35. This can be efficiently achieved via a propagator approach, using repeated matrix−vector multiplications, where the dimensions are set by the number of grid points used to partition the z-coordinate. We chose a grid spacing of 0.04σ and 0.02σ for polymer solutions and ideal polymer fluids, respectively. Several checks convinced us that these provided a sufficiently fine quadrature. In the absence of the angular potential (the fully flexible polymer model), the solution to eq 14 only requires us to store a two-dimensional matrix: the bond potential $\Theta(|\Delta z_k| - \sigma)$. With the semiflexible model, a three-dimensional, diagonally dominant matrix, $\Psi(\Delta z_l,\Delta z_{l+1})$, is also required.

Substitution of the equilibrium density into the free energy functional allows us to evaluate the grand potential, denoted by Ω_{eq}. From this quantity, we obtain the net solvation (surface) free energy per unit area, g_s, via a simple transformation:

$$g_s = \Omega_{eq}/S + P_b h \quad (17)$$

where P_b is the bulk pressure and S is the surface area. g_s will approach twice interfacial tension of the fluid at a single wall. We can generate the net solvation free energy by subtracting the limiting free energy:

$$\Delta g_s = g_s - g_s(h{=}\infty) \quad (18)$$

In our calculations, g_s at $h = \infty$ was satisfactorily approximated with its value at some large but finite separation.

The solvation pressure, P_s, can be calculated from the following derivative:

$$P_s = -\frac{\partial g_s}{\partial h} \quad (19)$$

or via the virial expression

$$P_s = -\int_0^h \sum_\alpha n_\alpha(z)\frac{\partial w_\tau^\alpha(h-z)}{\partial h}\,\mathrm{d}z - P_b \quad (20)$$

It is instructive to decompose the solvation pressure into contributions that act across the plane midway between the surfaces,[37] at $z = h/2$. The separate contributions are as follows: (i) A repulsive ideal entropic contribution, P_{en}, simply given by the total particle density at the midplane:

$$\beta P_{en} = n_m(h/2) + n_s(h/2) \quad (21)$$

(ii) A repulsive pressure, P_{coll}, due to collisions between particles on either side of the midplane. This term can be calculated from the excess part of the free energy. We begin by writing the excess free energy in the following, very general, form:

$$\beta\mathscr{F}^{ex} = \sum_\alpha \int_0^h n_\alpha(z) a_\alpha^{ex}(z)\,\mathrm{d}z \quad (22)$$

Using this expression, we obtain

$$\beta P_{coll} = -\sum_{\alpha}\sum_{\beta}\int_{\max(0,h/2-\sigma)}^{h/2}\int_{h/2}^{\min(z+\sigma,h)} n_\alpha(z)\, n_\beta(z')\frac{\partial\Theta(z'-z)}{\partial z'} \times \left\{\frac{\partial a_\alpha^{ex}(z)}{\partial n_\beta(z)} + \frac{\partial a_\beta^{ex}(z')}{\partial n_\beta(z)}\right\} \mathrm{d}z\, \mathrm{d}z' \quad (23)$$

where

$$\Theta(z'-z) = \frac{3}{4\sigma^3}(\sigma^2 - (z-z')^2) \quad (24)$$

is the coarse-graining kernel.

(iii) An attractive pressure, P_{acr}, due to particles on one-half of the midplane interacting with the wall on the other side

$$P_{acr} = -\sum_{\alpha}\int_0^{h/2} n_\alpha(z)\frac{\partial w_\alpha(h-z)}{\partial z}\,\mathrm{d}z \quad (25)$$

(iv) An attractive pressure, P_{bridge}, due to monomer−monomer bonds bridging across the midplane. For flexible chains, this is given by

$$\beta P_{br} = -2\sum_{i=1}^{r-1}\int_0^{h/2}\mathrm{d}z_i \int_{h/2}^{h}\mathrm{d}z_{i+1}\int_0^h \prod_{k\neq i,i+1}\mathrm{d}z_k\, N(z_1,z_2...z_r) \times \delta(z_{i+1}-z_i-\sigma_m) \quad (26)$$

For semiflexible polymers, the bridging expression is rather cumbersome. However, since all contributions add up to give the total solvation pressure

$$P_s = P_{en} + P_{coll} + P_{acr} + P_{br} - P_b \quad (27)$$

and all other contributions can be independently calculated from the above relations, we can obtain P_{br} implicitly from eq 27. *Net* bridging attractions (exceeding the bulk value) arise from polymer molecules that stretch between both surfaces, literally drawing them together. The attraction can be thought of as being due to the loss of configurational entropy that occurs as polymer molecules, adsorbed to both surfaces, are uncoiled when the surfaces are moved apart.

This partitioning provides us with some physical insight into the mechanisms responsible for the observed surface forces.

3. Results

In the presence of long polymer molecules, the surface free energy is affected at separations much greater than those where solvent structuring would manifest itself. At these separations, the interaction free energy is determined mainly by the behavior of polymer molecules. We expect that, as the molecular weight increases or the polymers becomes stiffer, effects are felt at larger separations. However, solvent structuring can still manifest indirectly via its influence on polymer adsorption at the surfaces.

3.1. Effect of Stiffness. In the presence of attractive surfaces, monomers will tend to bind cooperatively, leading to significant adsorption of polymer molecules. Acting against this is the loss in configurational entropy suffered by polymer molecules due to steric constraints imposed by the surfaces. Figure 1 shows the effect of increasing polymer stiffness on the adsorption of ideal polymer molecules. In this case the monomers are point particles, and there is no solvent. Interestingly, the monomer adsorption has a nonmonotonic dependence on the intrinsic chain stiffness. Starting with the fully flexible model ($\epsilon = 0$) and increasing the stiffness slightly ($\epsilon = 3$) causes the adsorption to decrease significantly. One can understand this behavior as follows. The entropic penalty paid by polymer molecules close to surfaces leads to a depletion of monomers within about $2R_g$ of the surface, where R_g is the radius of gyration. When the polymers becomes stiffer, angular correlations increase R_g, and the range of the depleted region increases. When the surface attraction is weak, some remnant of this effect is present. Increasing the stiffness to $\epsilon = 6$, however, causes the adsorption peak closest to the wall to increase again, and for $\epsilon = 12$, the monomer adsorption has become much greater than that of the flexible polymer fluid. This is due to the polymers adopting a more rodlike geometry, which increases the propensity for them to adsorb with flatter configurations, leading to a sharper adsorption peak close to the surface. Figure 2 displays two "snapshots" of typical configurations of ideal chains, which illustrate this effect. These were obtained from a simulation, but recall that ideal systems are treated *exactly* in the density functional theory. In one case we have a fully flexible ideal chain ($\epsilon = 0$) and in the other a slightly stiff ($\epsilon = 6$) chain. The impact of the stiffness parameter has on the intrinsic structure of a polymer is also clearly demonstrated in this figure.

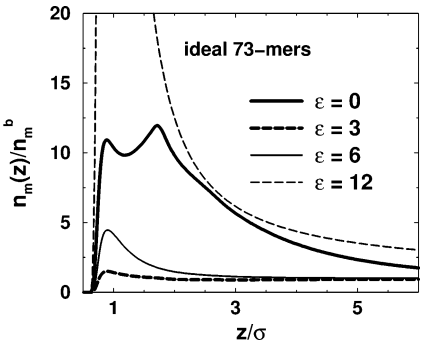

Figure 1. Monomer density profiles for ideal semiflexible 73-mers in a slit at separation $h/\sigma = 31$. Each curve displays the (exact) profile, as calculated with the indicated value of the intrinsic chain stiffness parameter ϵ. The strength of the surface potential is $A_w = 0.9$.

The effect on surface interactions upon stiffening the polymer molecules is shown in Figure 3. In the case of flexible polymers the interaction is predominately attractive at all separations. Investigation of the various pressure components across the midplane shows that the attraction is due primarily to polymer bridging. Bridging polymer molecules "coil up" when the surfaces are brought together, increasing the configurational entropy and thus lowering free energy. Counteracting this is a corresponding increase in the midplane density (i.e., the entropic force component, P_{en}). For the flexible case, the bridging component dominates this entropic repulsion at all separations. When polymers are made more stiff, they have a reduced tendency to coil, and the bridging component becomes weaker. The repulsive entropic term then dominates at larger surface separations. At shorter separations, however, bridging is still the major component. This leads to the formation of a free energy barrier, which increases with ϵ. When $\epsilon = 12$, we observe a very substantial free energy barrier due mainly to the high midplane density. Interestingly, increasing the stiffness even further exposes a nonmonotonic behavior in the free energy. The free energy barrier eventually disappears as the polymers become more rodlike. This limit warrants a separate investigation, which will be reported in a subsequent work.

We recall that in our solution model hard-sphere interactions occur between all species, and solvent and monomer particles

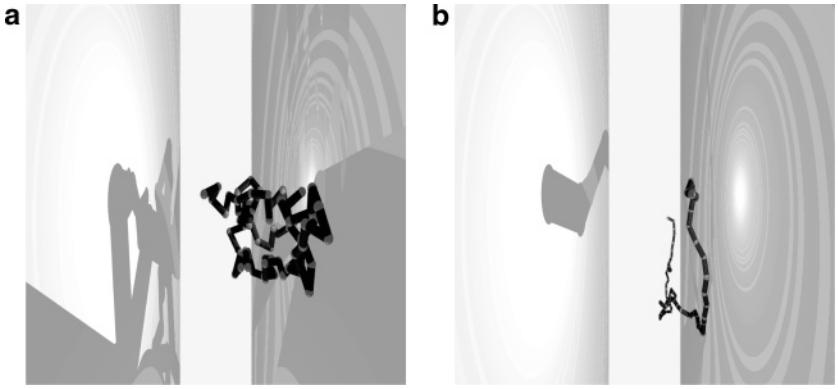

Figure 2. Configurational snapshots from a Metropolis Monte Carlo simulation of a single ideal 73-mer, in a slit confined by attractive surfaces, with $A_w = 0.9$. (a) Fully flexible chain: $\epsilon = 0$. (b) Semiflexible, with $\epsilon = 6$.

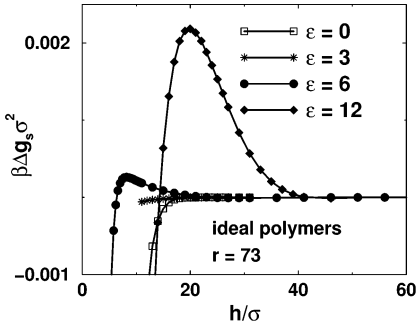

Figure 3. Influence of intrinsic chain stiffness on surface interaction free energies in ideal polymer fluids. The fluid contains ideal 73-mers, and the bulk monomer density is set to $n_m^b\sigma^3 = 0.1$, where σ is the bond length. The surface potential strength is the same as in Figure 1.

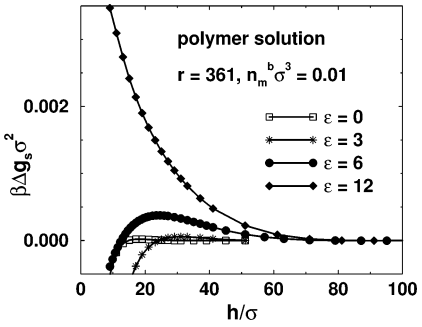

Figure 4. Influence of intrinsic chain stiffness on surface interaction free energies in athermal polymer solutions. The fluid contains 361-mers at a bulk monomer density of $n_m^b\sigma^3 = 0.01$. The bulk pressure is fixed at $\beta P_b\sigma^3 = 1.6904$, a condition that constrains the bulk solvent density to $n_s^b\sigma^3 \approx 0.5$. The hard-core diameter of monomers as well as solvent particles is equal to the bond length, σ. The adsorption potential acts equally on monomers and solvent particles, and its strength is characterized by $A_w = 2.7057$.

are equally attracted to the surfaces. Figure 4 shows the effect of increasing polymer stiffness, for the case $r = 361$, at a low bulk monomer density, $n_m^b\sigma^3 = 0.01$. The hard-sphere polymer solution model behaves similarly to the ideal case above. In the fully flexible case ($\epsilon = 0$), the surface interaction is mainly attractive, again due to bridging. Increasing the stiffness moderately, to $\epsilon = 3$, causes a small free energy barrier to form. The repulsive side of the barrier is due mainly to entropic and collisional contributions, P_{en} and P_{coll}, while the attractive part is due to bridging, which dominates at shorter separations. The barrier grows as the polymer is made even stiffer ($\epsilon = 6$). When $\epsilon = 12$, the surface interaction is essentially repulsive down to very short separations. In this case polymers are adsorbing on the surfaces with very flat orientations, and the "bridging-dominated regime" is now of such short range that it will be obscured by packing effects. This is not too surprising, since bridging now competes with the repulsive contributions, P_{en} and P_{coll}. These are furthermore coupled. Shorter polymers, with the same stiffness parameter, should show similar qualitative behavior, whereas a free energy barrier may be reestablished for longer chains. We investigate this in the next section.

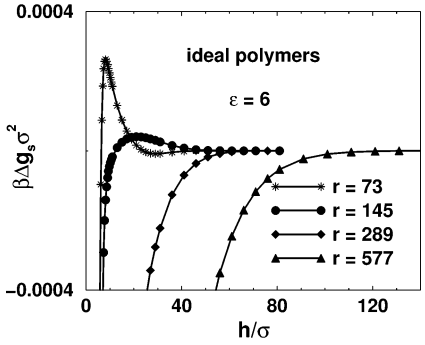

Figure 5. Influence of chain length on surface interaction free energies in semiflexible ideal polymer fluids. The intrinsic stiffness parameter is fixed at $\epsilon = 6$, which generates a persistence length of about 6σ. The surface potential and the bulk conditions were identical to those in Figure 3.

3.2. Molecular Weight Dependence. In Figure 5, we show effects of increasing the chain length of an ideal polymer fluid. We emphasize that all results reported for ideal chains are *exact*. The internal stiffness of the polymer molecules is fixed, with $\epsilon = 6$. Here we note that, as the chains become longer, the interaction displays a weaker free energy barrier. As discussed previously, the barrier is due to a change in dominance between repulsive entropic and attractive bridging contributions. Hence, as the chain length increase, the bridging component has a longer range and the repulsive contributions become relatively smaller. Thus, the barrier reduces as the surface interaction is dominated by attractive bridging.

Figure 6a shows the surface interaction in polymer solutions at a relatively low bulk monomer concentration, $n_m^b\sigma^3 = 0.01$. As the molecular weight is changed, we find the same qualitative behavior as in the ideal fluid. The barrier is in the solution model due to entropic and collisional contributions, with bridging interactions dominating at short separation. As was the case for the ideal solutions, the barrier becomes smaller and occurs at larger separations as the molecular weight increases. The shorter the polymer, the more stiff it is across its length. This causes the bridging component to decrease, and thus the barrier becomes larger. These arguments suggest that we should be able to obtain significant and long-ranged barriers also with longer chains, provided the intrinsic stiffness is increased sufficiently.

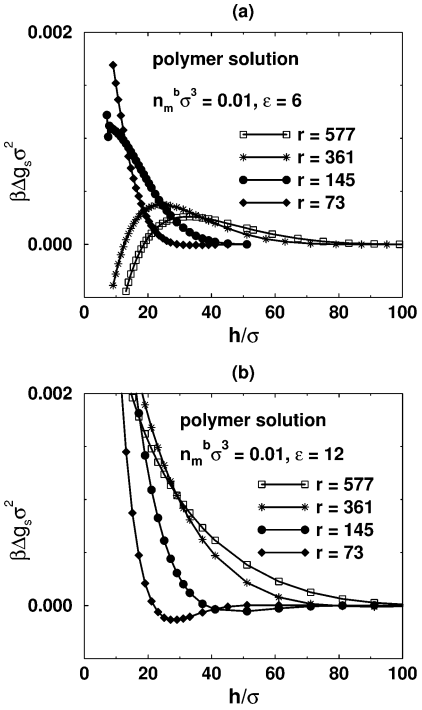

Figure 6. Influence of chain length and intrinsic stiffness on surface interaction free energies in athermal polymer solutions, at $n_m^b\sigma^3 = 0.01$. The bulk pressure and surface potential strength are the same as in Figure 4. (a) Stiffness parameter: $\epsilon = 6$. (b) Stiffness parameter: $\epsilon = 12$.

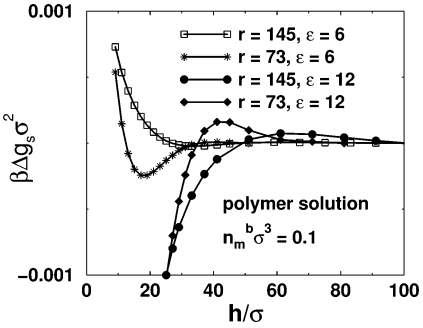

Figure 7. Influence of chain length and intrinsic stiffness on surface interaction free energies in athermal polymer solutions, at $n_m^b\sigma^3 = 0.1$. The bulk pressure and surface potential strength are the same as in Figure 4. This constraint results in a bulk solvent density of about $n_s^b\sigma^3 \approx 0.431$.

This is demonstrated in Figure 6b. Note the onset of a minimum prior to the attractive regime, for the shortest chain. This is related to saturation effects and the approach to rodlike behavior. This will be briefly discussed below and more thoroughly investigated in a separate work.

3.3. Effect of Monomer Concentration. Finally we consider the effect of increasing the monomer concentration. In the previous sections, the monomer density in the polymer solution was fixed at $n_m^b\sigma^3 = 0.01$. In Figure 7, we present the interaction free energy that results from a 10-fold increase of the bulk monomer density, while maintaining the total bulk pressure of the solution at its prescribed value, $\beta P_b\sigma^3 = 1.6904$. It is apparent that the concentration increase causes the surface interactions to become shorter ranged for both flexible and stiff polymers. This is to be expected on the basis of a density-dependent bulk correlation length, which becomes smaller as the concentration increases.[12] Interestingly, the midplane force contributions display *completely* different behaviors for the

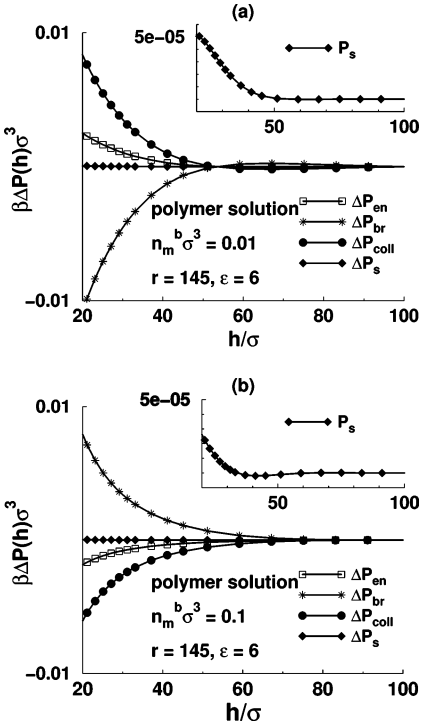

Figure 8. Analysis of the separate pressure contributions for a 145-mer polymer solution at two different bulk monomer densities, at $\beta P_b\sigma^3 = 1.6904$. The chain stiffness is characterized by $\epsilon = 6$, and the surface potential strength is the same as in Figure 4. The corresponding pressure contributions in the bulk have been subtracted, i.e., $\Delta P_\alpha = P_\alpha(h) - P_\alpha(h_{max})$, where h_{max} is a large separation. The inset gives the net pressure, in each case. (a) Monomer density: $n_m^b\sigma^3 = 0.01$. (b) Monomer density: $n_m^b\sigma^3 = 0.1$.

various contributions as the density increases (see Figure 8). At high monomer concentrations, polymers are being depleted from the slit, leading to net attractive entropic and collisional contributions. This change in behavior comes about due to a saturation in the amount of polymer adsorbed at the higher concentration. The large adsorption precludes other interstitial molecules from interacting favorably with the surfaces. As polymers are being depleted, the total bridging attraction will naturally be weaker (fewer bridges), i.e., when compared with its bulk value, there is a *net repulsive* bridging interaction. Furthermore, the net repulsive bridging contribution dominates the depletion attraction, leading to a repulsive interaction. This implies that polymers are either being compressed by, or aligned with, the surfaces, which reduces the strength of the bridging attraction, as measured *per chain*.

4. Conclusion

We have investigated the free energy of interaction between attractive surfaces, which confine solutions containing semiflexible polymer molecules. In the Appendix, it is verified that the density functional theory we have used accurately predicts structural properties of solutions containing semiflexible polymers. Effects of varying stiffness, chain length, and polymer concentration have been considered in this study. A significant result is the discovery of an enormous increase in the barrier to surface association, upon increasing the degree of stiffness of the polymer molecules. Thus, deviations from the de Gennes prediction of monotonically attractive surface free energies become greater, with increasing stiffness. Our results do suggest, however, that the de Gennes result may be realized in the limit of infinite chain length. That is, the free energy barriers decrease with increasing molecular weight, for a given intrinsic chain

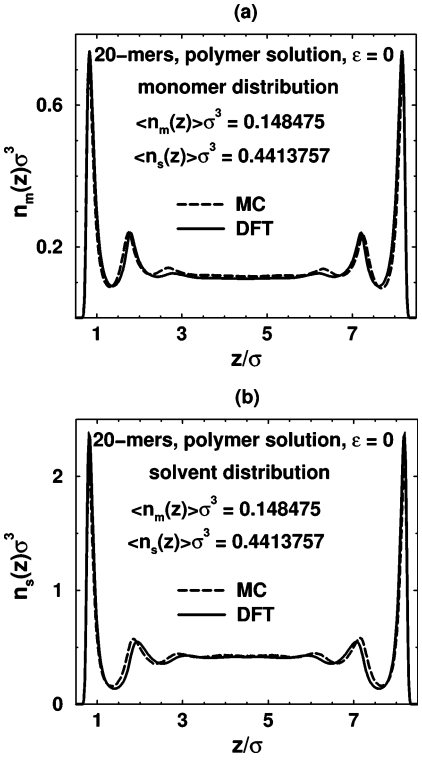

Figure 9. Density distributions in an athermal 20-mer solution, containing fully flexible ($\epsilon = 0$) chains and an explicit representation of the hard-sphere solvent. σ is the hard-sphere radii, common to monomers and solvent particles, and is also the bond length between connected monomers in a chain. Monomer and solvent densities are denoted by n_m and n_s, respectively. "DFT" denote density functional predictions, while "MC" are results from canonical Metropolis Monte Carlo simulations. (a) Monomer distributions. (b) Solvent particle distributions.

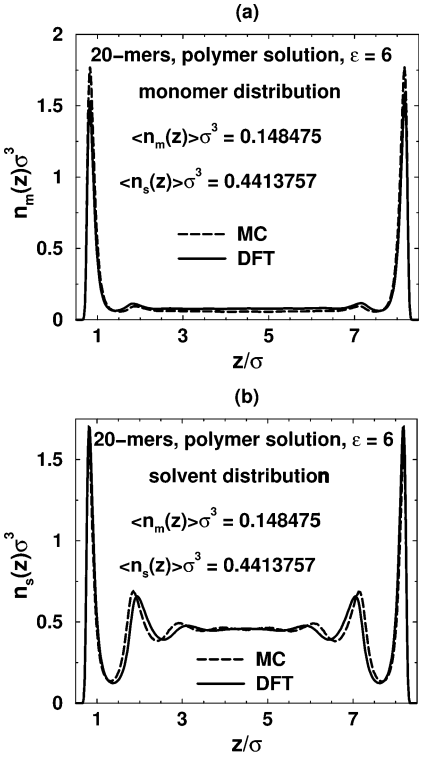

Figure 10. Density distributions, as described in Figure 9, but for a solution containing semiflexible polymers: $\epsilon = 6$. (a) Monomer distributions. (b) Solvent particle distributions.

stiffness. An advantage of the analysis we present here is the ability to discriminate separate contributions to the surface interactions, in particular the relative roles played by bridging, entropic, and collisional terms to the osmotic pressure. This has allowed us to reveal a surprising reversal of the mechanisms responsible for surface interactions, given an increase in polymer concentration. At low concentrations, attractions between surfaces are caused by bridging interactions, while repulsions are due to entropy decreases related to confinement as well as hard-core collisions. However, an order of magnitude increase in polymer density (at constant bulk pressure) causes surface interactions to be attractive at long range, due to polymer depletion, and repulsive at short range, due to compression or alignment of polymers. This illustrates that surface forces mediated by polymers are not simply proportional to the monomer concentration. Changes in concentration can give rise to completely different interaction mechanisms, which only become elucidated through detailed theoretical investigations of the type reported in the present work.

Appendix

Here, we shall make structural comparisons between density functional predictions and corresponding results obtained by standard canonical Metropolis Monte Carlo simulations. These are briefly described as follows: each chain contains 20 monomers. We have only considered two types of polymers: fully flexible ($\epsilon = 0$) and semiflexible ones. In the latter case, the intrinsic chain stiffness potential was included, with $\epsilon = 6$. We have adopted the same surface potential as in the density functional studies described above; i.e., it acts equally on monomers and solvent particles (with $A_w \approx 2.7057$). Average particle densities are calculated over the allowed regions between the surfaces, i.e., within 0.5σ from each wall. Specifically, we performed all simulations at $h = 9\sigma$, with the average monomer density given by

$$\langle n_m(z)\rangle_{0.5\sigma,h-0.5\sigma} \equiv \frac{\int_{0.5\sigma}^{h-0.5\sigma} n_m(z)\,\mathrm{d}z}{h-\sigma} = 0.148475 \quad (28)$$

Analogously, the average solvent density was $\langle n_s(z)\rangle_{0.5\sigma,h-0.5\sigma} = 0.4413757$. The standard Metropolis[38] algorithm was employed, with periodic boundary conditions applied in the lateral directions parallel with the surfaces. The lateral dimension of the simulation box was $L \approx 19.25\sigma$. Attempts to displace the polymer and monomer particles were made via crankshaft moves or translations of the whole chain. 12% of the attempted moves were devoted to solvent translations. Note that the total volume fraction is relatively high, which amounts to a critical test of the approximate equation of state,[22,34] which enters the density functional theory.

Comparisons of monomer and solvent density profiles for fully flexible chains are given in Figure 9. The theory underestimates the third monomer density peak, and there is a small phase lag in the solvent density oscillations, but overall the agreement is very good. Figure 10 shows that the profiles in a solution containing semiflexible polymers (with $\epsilon = 6$) are also well reproduced by the theory, although the primary monomer density peak is somewhat underestimated.

A comparison between Figures 9 and 10 clearly demonstrates the increased adsorption of the stiffer chains and, furthermore, that the higher adsorption will cause solvent molecules to be expelled from the surfaces. These behaviors are clearly well captured by the functional.

In summary, the density functional theory is able to make accurate predictions of structural properties in solutions contain-

ing flexible as well as semiflexible polymers. This provides strong support for the overall findings on surface interactions in such systems, as outlined in this work.

References and Notes

(1) Patel, S. S.; Tirrell, M. *Annu. Rev. Phys. Chem.* **1989**, *40*, 597.
(2) Hu, H.-W.; Granick, S. *Macromolecules* **1990**, *23*, 613.
(3) Ruths, M.; Yoshizawa, H.; Fetters, L. J.; Israelachvili, J. N. *Macromolecules* **1996**, *29*, 7193.
(4) Kuhl, T.; Guo, Y.; Alderfer, J. L.; Berman, A. D.; Leckband, D.; Israelachvili, J. N.; Wen Hui, S. *Langmuir* **1996**, *12*, 3003.
(5) Kuhl, T.; Berman, A. D.; Wen, H. S.; Israelachvili, J. N. *Macromolecules* **1998**, *31*, 8250.
(6) Kuhl, T.; Berman, A. D.; Wen, H. S.; Israelachvili, J. N. *Macromolecules* **1998**, *31*, 8258.
(7) Seitz, M.; Park, C. K.; Wong, J. Y.; Israelachvili, J. N. *Langmuir* **2001**, *17*, 4616.
(8) Asakura, S.; Oosawa, F. *J. Chem. Phys.* **1954**, *22*, 1255.
(9) Asakura, S.; Oosawa, F. *J. Polym. Sci.* **1958**, *33*, 183.
(10) Vrij, A. *Pure Appl. Chem.* **1976**, *48*, 471.
(11) Joanny, J.-F.; Leibler, L.; deGennes, P. G. *J. Polym. Sci., Polym. Phys. Ed.* **1979**, *17*, 1073.
(12) deGennes, P. G. *Macromolecules* **1981**, *14*, 637.
(13) deGennes, P. G. *Macromolecules* **1982**, *15*, 492.
(14) Feigin, R. I.; Napper, D. H. *J. Colloid Interface Sci.* **1980**, *74*, 567.
(15) Feigin, R. I.; Napper, D. H. *J. Colloid Interface Sci.* **1980**, *75*, 525.
(16) Scheutjens, J. M. H. M.; Fleer, G. J. *Macromolecules* **1985**, *18*, 1882.
(17) Woodward, C. E. *J. Chem. Phys.* **1992**, *97*, 695.
(18) Semenov, A. N.; Joanny, J.-F. *Europhys. Lett.* **1995**, *29*, 279.
(19) Bonet-Avalos, J.; Joanny, J.-F.; Johner, A.; Semenov, A. N. *Eurpohys. Lett.* **1996**, *35*, 97.
(20) Broukhno, A.; Åkesson, T.; Jönsson, B.; Vorontsov-Velyaminov, P. *J. Phys. Chem. Phys.* **2000**, *113*, 1.
(21) Czezowski, A. Thesis, ADFA, Canberra, 2001.
(22) Forsman, J.; Woodward, C. E.; Freasier, B. C. *J. Chem. Phys.* **2002**, *117*, 1915.
(23) Forsman, J.; Woodward, C. E.; Freasier, B. C. *J. Chem. Phys.* **2003**, *118*, 7672.
(24) Forsman, J.; Woodward, C. E. *J. Chem. Phys.* **2004**, *120*, 506.
(25) Woodward, C. E.; Forsman, J. *Macromolecules* **2004**, *37*, 7034.
(26) Edwards, S. F. *Proc. R. Soc. London* **1965**, *85*, 613.
(27) Blokhuis, E. M.; Skau, K. I. *J. Chem. Phys.* **2003**, *119*, 3483.
(28) van der Linden, C. C.; Leermarkers, A. M.; Fleer, G. J. *Macromolecules* **1996**, *29*, 1172.
(29) Sintes, T.; Sumithra, K.; Straube, E. *Macromolecules* **2001**, *34*, 1352.
(30) Semenov, A. N. *Eur. Phys. J. E* **2002**, *9*, 353.
(31) Mishra, P. K.; Kumar, S.; Singh, Y. *Physica A* **2003**, *323*, 453.
(32) Forsman, J.; Woodward, C. E. *J. Chem. Phys.* **2003**, *119*, 1889.
(33) Yethiraj, A.; Woodward, C. E. *J. Chem. Phys.* **1995**, *102*, 5499.
(34) Wichert, J. M.; Gulati, H. S.; Hall, C. K. *J. Chem. Phys.* **1996**, *105*, 7669.
(35) Woodward, C. E. *J. Chem. Phys.* **1991**, *94*, 3183.
(36) Nordholm, S.; Johnson, M.; Freasier, B. C. *Aust. J. Chem.* **1980**, *33*, 2139.
(37) Miklavic, S. J.; Woodward, C. E. *J. Chem. Phys.* **1990**, *93*, 1369.
(38) Metropolis, N. A.; Rosenbluth, A. W.; Rosenbluth, M. N.; Teller, A.; Teller, E. *J. Chem. Phys.* **1953**, *21*, 1087−1097.

MA051934G